What happens in the soil during pile driving?

by ir G. DE JOSSELIN DE JONG[1]
Delft Soil Mechanics Laboratory

Summary: What happens in the soil during pile-driving?

A. A graphical method is used to determine stress and velocity in rods under dynamic loading conditions. Application to a sample of dry sand gives regions of permanent deformation and dissipation of energy into friction. Penetration of the energy into the interior of the sample is deeper for longer duration of impact. Experiments confirm this theoretical result.

B. The way sand saturated with water reacts on dynamic load is studied by separating stresses and velocities of the two phases. It is shown that water bears nearly total dilatation stress, while the granular skeleton is affected by rotation for high frequency loading.

C. Impedance of rigid sphere in infinite, elastic medium is computed in order to obtain information about the impedance of a pile-toe in soil. It is shown that for high frequencies the load is mostly affecting the water stresses. The different effects of these phenomena on the reaction of a pile while driven into the soil are considered.

Introduction

If one wonders what happens in the soil during pile driving, one encounters a phenomenon of a dynamic nature, the description of which currently cannot be given in a closed mathematical form. In this article we will try to review the different aspects of this phenomenon one at a time to facilitate further examination from both a practical and a theoretical angle.

When the compression wave, generated by the impact of the ram on the pile cap, reaches the toe after travelling through the pile, part of the compression wave extends into the surrounding soil mass and the remainder returns through the pile as un upward wave.

First, we will use the method of characteristics to give an indication of the effects developing in the pile when it is impacted by the falling ram. We will also demonstrate how the response of a material, such as sand with irreversible deformation properties, to an impact load can be formulated by consistently applying this method. The derived results relate primarily to cylinders of dry sand.

Next the question arises how a stress wave propagates in a mixed medium such as soil, which consists of granules and water. The problem can be solved by assigning linear deformation properties to the granular skeleton. Although this does mean an idealization of the soil, the solution makes it possible to draw general conclusions. This will also allow to describe the distribution of the forces between the two phases: granules and water.

Finally, we will describe the propagation of a stress wave in the idealized soil mass around a pile toe, whereby a geometric schematization (representing the pile toe by a rigid sphere) is necessary to allow for a mathematical solution. Once the three-dimensional character of the

[1] The contributors to the translation of this paper are Peter Middendorp (Allnamics), Gerald Verbeek (Allnamics USA), and Ryan van der Eijk (Boskalis)

stress wave propagation has been obtained in this way, it is again possible to calculate the distribution of the forces between the two phases.

By combining the various results, it is possible to demonstrate certain tendencies, which may be useful in the examination of more practical issues, such as the magnitude of the stresses that can be expected in a pile during pile driving as well as the relationship between the soil behaviour during pile driving and the bearing capacity of the pile under static loading.

A. Propagation of a stress wave

The mathematical model of the wave propagation in elastic rods was already developed by de Saint Venant, and applied in a logical manner by Nanninga [1] to address a pile-driving issue. However, to examine what happens when materials with non-linear irreversible stress-deformation properties (here the soil underneath the pile toe come to mind immediately) exert their influence during pile-driving, the mathematical model is no longer adequate. Only a graphical method, such as the method of characteristics[2] is then suitable. Since this method is not yet widely known, the approach will be described in the following paragraphs, starting with elementary concepts, so that afterwards it can be applied to sand.

When considering the stress wave propagation in rods, the two d'Alembert equations are used. These two basic equations describe the inertia and continuity of a rod segment with a length of *dx* and cross-section *F* (Fig. 1), and relate the variables pressure *P*, velocity *V*, distance *x* and time *t*.

The mass of the segment $\varrho F dx$ undergoes an acceleration as a result of the force exerted on the segment $-\left(\frac{\delta P}{\delta x}\right) dx$ in the x-direction, so that Newton's law after division by dx reads:

$$\varrho F \frac{\delta V}{\delta t} = -\frac{\delta P}{\delta x} \qquad (1)$$

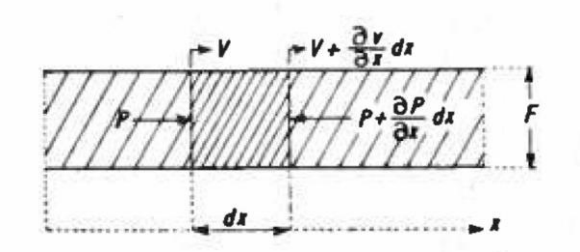

Figure 1: Stress and velocity of rod segment

The continuity of matter requires that the shortening Δdx of segment dx due to the different velocities of the front face and back face corresponds with the compressive force *P* and the compressibility of the rod. Application of Hooke's law yields *P/EF = (Δdx)/dx*. During time interval *dt* the force increases by *(dP/dt)dt* and the shortening by *[d(Δdx)/dt]dt*, which can be restated as *–(dV/dx)dxdt*, because *d(Δdx)/dt* is equal to the velocity difference between the front and back face of dx. Hooke's law therefore yields:

$$\left(\frac{1}{EF}\right)\frac{\delta P}{\delta t} = -\frac{\delta V}{\delta x} \qquad (2)$$

The relationship between *P, V, x* and *t* is best understood by multiplying eq. (1) by $\sqrt{E/\varrho}$ and then adding it to or subtracting it from eq. (2) multiplied by (EF). The outcome is then:

$$\pm\left(F\sqrt{E\varrho}\frac{\delta V}{\delta t} \pm \frac{\delta P`}{\delta t}\right) + \left(FE\frac{\delta V}{\delta x} \pm \sqrt{\frac{E}{\varrho}}\frac{\delta P}{\delta x}\right) = 0$$

or

$$\left(\sqrt{\frac{E}{\varrho}}\frac{\delta}{\delta x} \pm \frac{\delta}{\delta t}\right)\left(F\sqrt{E\varrho}\,V \pm P\right) = 0 \qquad (3)$$

[2] This method has been developed by Massau [2] and applied by among others Schönfeld [3] in hydraulics. For an extensive description of the method see e.g., Sauer [4].

Let us first deal with the operator

$$\left[\sqrt{\frac{E}{\varrho}}\left(\frac{\delta}{\delta x}\right) \pm \left(\frac{\delta}{\delta t}\right)\right]$$

This can be simplified when focusing on the various states of the rod, which during time interval *dt* travels along the rod by

$$\pm\delta x = \sqrt{\frac{E}{\varrho}}\,\delta t \qquad (4)$$

In other words, the area of interest moves with a velocity of $\sqrt{E/\varrho}$ (cm/sec) along the rod in positive (or negative) direction. After multiplying by *dt* this operator then simplifies to a total differential equation:

$$\delta t\left(\sqrt{\frac{E}{\varrho}}\frac{\delta}{\delta x} \pm \frac{\delta}{\delta t}\right) = \pm\left(dx\frac{\delta}{\delta x} + dt\,\frac{\delta}{\delta t}\right)$$

which means that eq. (3) can be written as

$$\pm\left(dx\frac{\delta}{\delta x} + dt\,\frac{\delta}{\delta t}\right)\left(F\sqrt{E\varrho}\,\boldsymbol{V} \pm P\right) =$$

$$= \pm d\left(F\sqrt{E\varrho}\,V \pm P\right) = 0 \qquad (5)$$

Integration is then simple and results in

$$P \pm F\sqrt{E\varrho}\,V = constant \qquad (6)$$

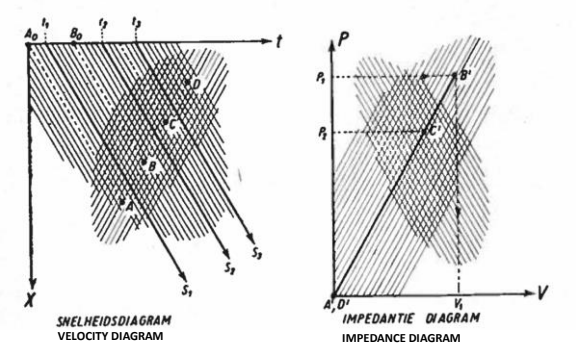

Figure 2:. For discontinuous stress variations, a specific situation in the velocity diagram is represented by a specific point in the impedance diagram

So eq. (6) states that when monitoring changes in *P* and *V* while moving along the x-axis at a velocity $\pm\delta x/\delta t = \sqrt{E/\varrho}$, any increase in *P* results in a change in velocity according to the ratio $\frac{dP}{dV} = \pm F\sqrt{E\varrho}$.

In physics the ratio $Z = F\sqrt{E\varrho}$ is commonly referred to as the impedance of the rod and the more the impedance *Z* increases the stiffer the rod behaves under dynamic conditions.

A I. Method of Characteristics

Eqs. (4) and (6) form the basis of the method of characteristics, which is particularly suitable for the examination of discontinuous phenomena.

This method displays graphically the relationship between *P, V, x* and *t* using two diagrams: the first with coordinates *x* and *t*, the velocity diagram; and the other with coordinates *P* and *V,* the impedance diagram. Figure 2 shows these diagrams for a rod that is loaded at *x = 0* by *P* = 0 for $t < t_1$ *and* $t_3 < t$ and $P = P_1$ for $t_1 < t < t_2$ and $P = P_2$ for $t_2 < t < t_3$.

In the graphs the characteristic lines are drawn, with slope $\delta x/\delta t = \pm\sqrt{E/\varrho}$ in the velocity diagram and $dP/dV = \pm F\sqrt{E\varrho}$ in the impedance diagram. For any characteristic line, e.g., the line A_oA with slope $\delta x/\delta t = +\sqrt{E/\varrho}$, the sum $P + F\sqrt{E\varrho}\,V$ is constant along that line. For *x = 0* it is given that *P = 0*. If we also assume that the rod is initially at rest, or *V = 0*, then the state along the line A_oA is defined by the origin of the impedance diagram, i.e., the point *A'*. This state remains the same along the entire line A_oA and thus also for point A. Let us now consider a second characteristic line B_oB. At the place where this line intersects the x = 0 axis there is a pressure P_1 and as yet unknown velocity V_1, which we can derive by starting from the state at point A. To do this we must go from A to B along a characteristic line with slope $\delta x/\delta t =$

$-\sqrt{E/\varrho}$. The foregoing yields that along such a line the difference $P - F\sqrt{E\varrho}\,V$ is constant, which means that in the impedance diagram it is positioned somewhere on a characteristic line that runs through A' with slope $dP/dV = +F\sqrt{E\varrho}$. The position of B' in the impedance diagram is then derived by intersecting this characteristic line with the line for $P = P_1$, which means that the position of B' also defines the value of V_1. In the same manner the points C' and D' can be derived from the location of points C and D in the velocity diagram. Since we have assumed a constant load P_1 for the time interval $t_1 - t_3$, point B' in the impedance diagram applies to the entire interval in the velocity diagram and also to the entire area that extends slanting to the bottom right. Thus, an area in the velocity diagram is mapped as a point in the impedance diagram when the pressure variations are discontinuous.

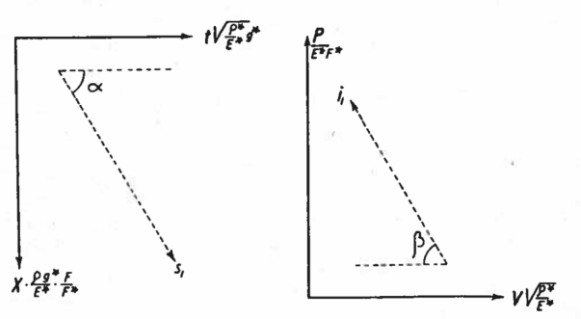

Figure 3: Characteristic lines with dimensionless scales so that the lines run parallel

When line S_1 is crossed while moving along the line ABCD starting at point A, then the state abruptly changes from A' to B' in the impedance diagram, remains B' until line S_2 is crossed, at which time it changes to C' etc. These abrupt transitions are of course smooth in reality.

A 2. Choice of scales

Since characteristic directions occur in the diagrams, it is attractive to choose the scales of the diagrams in such a way that the corresponding directions are parallel. This can be achieved by entering arbitrary reference units: a density ρ^* (kg/m^3), a modulus of elasticity E^* (N/m^2), a cross sectional area F^* (m^2) and an acceleration g^* (m/sec^2) and thus compose the following dimensionless coordinate units:

$$x.\frac{F\varrho g^*}{E^*F^*} \qquad tg^*\sqrt{\varrho^*/E^*} \qquad \frac{P}{E^*F^*} \qquad V.\sqrt{\frac{\varrho^*}{E^*}}$$

In doing so the angle α between the characteristic line S_1 in the velocity diagram of Fig. 3 and the time axis is defined as

$$tg\,\alpha = \frac{dx}{dt}\cdot\frac{\varrho g^*}{E^*}\cdot\frac{F}{F^*}\cdot\frac{1}{g^*}\sqrt{\frac{E^*}{\varrho^*}}$$

which, when combined with eq. (4), can be rewritten as

$$tg\,\alpha = \pm\frac{F\sqrt{E\varrho}}{F^*}\sqrt{E^*\varrho^*} \qquad (7)$$

Similarly, in the impedance diagram the slope β of the characteristic line l1, is defined as

$$tg\,\beta = -\frac{dP}{dV}\cdot\frac{1}{E^*F^*}\sqrt{\frac{E^*}{\varrho^*}}$$

which, when combined with eq. (4), can be rewritten as

$$tg\,\beta = \pm\frac{F\sqrt{E\varrho}}{F^*}\sqrt{E^*\varrho^*} \qquad (8)$$

This shows the desired outcome that $\alpha = \beta$.

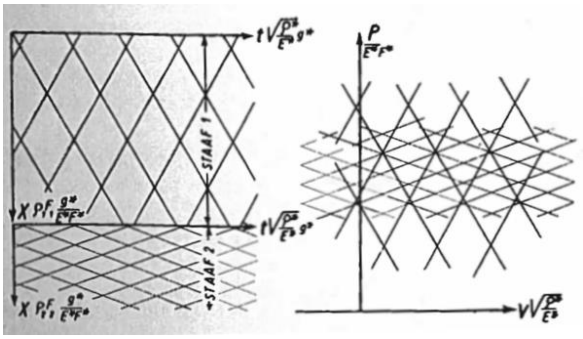

Figure 4: When two bars are connected to each other, their characteristic lines mix in the impedance diagram, but are separated in the velocity diagram. By applying dimensionless scales, the same mass per unit length is present along the x-axis

From eqs. (7) and (8) it is evident the tangents of the characteristic lines are directly proportional to the impedance $Z = F\sqrt{E\varrho}$.

When two rods of different material and cross-section are connected to each other, their characteristic directions form two intermixing networks in the impedance diagram (Fig. 4). As long as the bars touch each other, the force and the velocity at the common cross-section are equal, so that that state is indicated by one and the same point in the impedance diagram.

However, in the velocity diagram the two rods are separated in the direction of the x coordinate. The scale of this coordinate varies with the value of ρ and *F* for the rod in question, contrary to the scales of the other coordinates *t, P* and *V,* which only contain the reference units. The scale of x must therefore be adapted to the ρF of the rods, which results in the fact that there is the same amount of rod mass per unit length of the x-coordinate. Due to the difference in the characteristic direction in each of the rods, the velocity diagram consists of two parts, each with its own characteristic network (Fig. 4).

In order to avoid any misunderstanding, it should be pointed out here that the x-coordinate is related to the rod itself and not to the special position of the rod in space.

A 3. Energy

The kinetic and potential energies present in each unit length of the rod can be stared as

$$w = \frac{1}{2}\, F\varrho\, V^2 + \frac{\frac{1}{2}P^2}{EF} \qquad (9)$$

Therefore the lines that connect points in the impedance diagram with equal amounts of energy per unit volume are ellipses (see Fig. 5) with major axes

$$P = \sqrt{2wEF} \text{ and } V = \sqrt{\frac{2w}{\varrho F}}$$

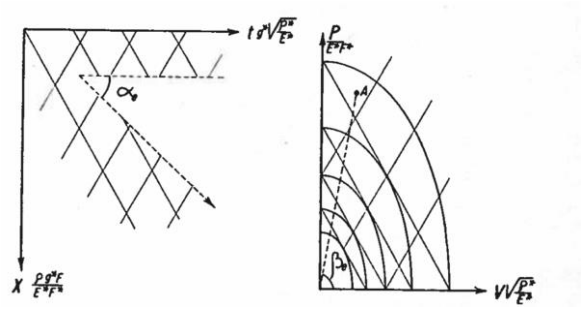

Figure 5:. The velocity, with which energy is transmitted, occurs at a slope α_e, which differs from the characteristic slope α in the velocity diagram.
In the impedance diagram, ellipses connect the points of equal energy

The energy transmission velocity is determined as follows:

- the amount of energy transmitted during dt in a cross section is $dw = V.P\ dt$
- this quantity is distributed over a distance *dx* whereby $dw = \left(\frac{1}{2}F\varrho V^2 + \frac{\frac{1}{2}P^2}{EF}\right)dx$
- therefore the energy transmission velocity is

$$\frac{dx}{dt} = \frac{2PV}{F\varrho V^2 + \frac{P^2}{EF}} \qquad (10)$$

This velocity can be represented in the velocity diagram by a line with a slope α_e, which does not need to correspond with the characteristic velocity direction when we consider an arbitrary state *P,V* (represented by point *A* in Fig. 5).

The angle β_e, at which A is seen from the origin of the impedance diagram, can be stated as

$$tg\ \beta_e = \frac{P}{V}\ F^*\sqrt{E^*\varrho^*}$$

While based on eq. (10) α_e can defined as

$$tg\ \alpha_e = \frac{dx}{dt}\cdot\frac{\varrho F}{F^*\sqrt{E^*\varrho^*}} = \frac{\frac{2P}{V}\ F^*\sqrt{E^*\varrho^*}}{\left[1 + \frac{P^2}{V^2}\ \mathrm{F}^2 E\varrho\right]}$$

Based on eq. (7) the characteristic slope α is defined as

$$tg\ \alpha_e = \frac{2\ tg\ \beta_e}{\left[1+\left(\frac{tg^2\beta_e}{tg^2\alpha}\right)\right]} \qquad (11)$$

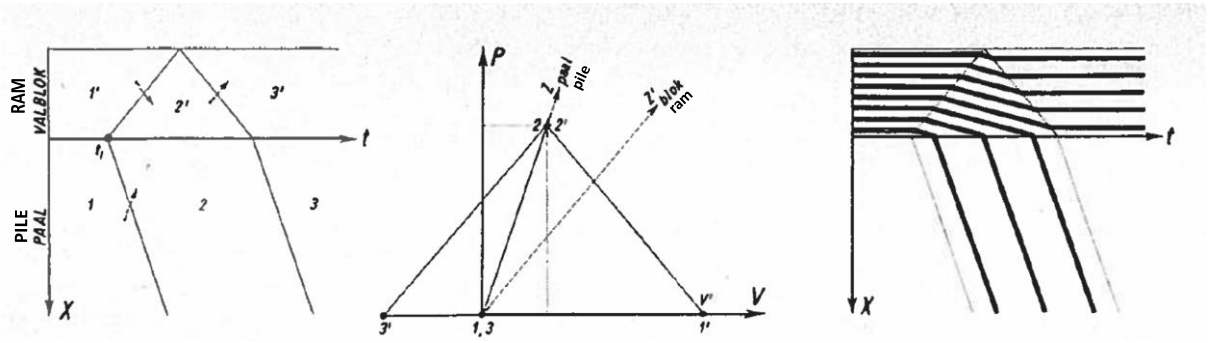

Figure 6a. Small ram impacts large pile. The ram rebounds

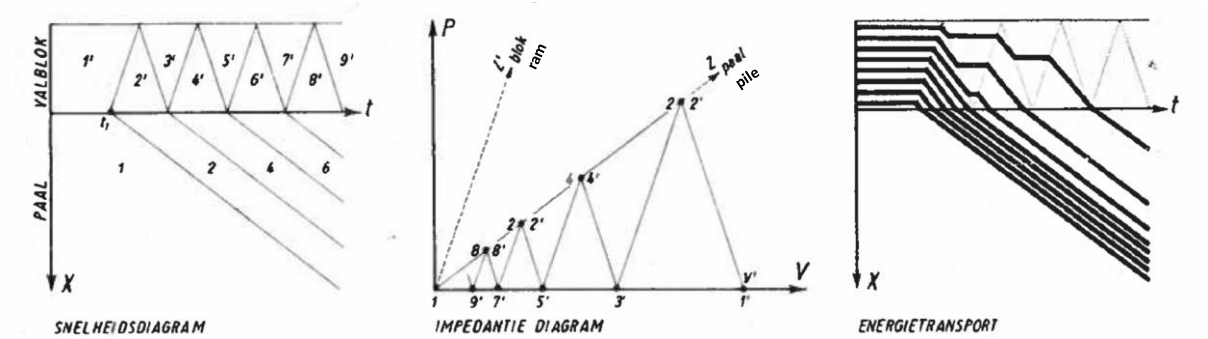

Figure 6b: Large ram impact small pile. The ram keeps pushing and does not rebound

This shows for example, that $\alpha_e = 0$ for $\beta_e = 0$ and $\beta_e = \pi/2$, which means that there is no energy transmission in a rod that is under static pressure ($V = 0$) or in which there is no stress ($P = 0$).

A 4. Application of the characteristics

The use of the characteristics may be illustrated with two examples, starting with a drop hammer that strikes the top of a pile (Fig. 6), and then the progression of a stress wave through the pile, which encounters a solid with a different stiffness at the pile toe (Fig. 7).

As shown in the Fig. 6, the drop hammer falls at a velocity V^1 to encounter a pile, which is either stiffer (Fig. 6a) or less stiff (Fig. 6b). In the first case, the pile impedance (Z) is greater than that in the ram (Z') and therefore the pile characteristic angle in the impedance diagram is steeper, while in the second case the pile impedance is smaller.

The derivation of the pressure and velocity is now as follows. As can be seen in the velocity diagram, at *t1* the drop hammer impacts the pile. From that moment on a compression wave travels downwards through the pile and upwards in the ram at propagation velocities, which are given by the characteristic angles in both media. Prior to t_1 the drop hammer was in state 1' ($P = 0$, $V = V^1$) and the pile in state 1 ($P = 0$, $V = 0$) represented by points 1' and 1 in the impedance diagram.

From t_1 onwards, the drop hammer and the pile are in contact with each other and thus have equal stress and velocity, i.e., the state in regions 2 and 2' in the velocity diagram are represented by one and the same point in the impedance

diagram. This point is determined by drawing in the velocity diagram a line through point 1' with the same angle as the characteristic that must be followed to get from area 1' to area 2' (the dotted arrow). The process is repeated for 1. The intersection of these lines is a point designated as 2',2 in the impedance diagram. Next the stress wave in the drop hammer reaches the top, which must of course be stress-free. This is achieved as a second wave runs down the drop hammer, delineating area 3'. The transition from 2' to 3' in the velocity diagram along the characteristic line (the dashed arrow) produces in case of the stiffer pile (Fig. 6a) point 3' in the impedance diagram that indicates a negative velocity, which means that the drop hammer will bounce back. In case of a pile that is not as stiff as the drop hammer, the drop hammer velocity in region 3 remains positive, indicating that the ram continues to apply pressure on the pile top, thus generating another stress wave 4' in the pile with less pressure and so on in a descending geometric sequence. The end result is then that the ram remains on the pile (Fig. 6b).

In Fig.6 the velocity diagram is repeated on the right side to show the energy transmission velocity. Each line represents a certain amount of energy, and the line pattern indicates where the energy remains (with the line spacing designating the energy density). The construction of the respective directions follows from an application of eq. (11).

Figure 7 shows what occurs when a stress wave, which is generated by a falling drop hammer as illustrated in Fig. 6a, reaches the pile toe after having travelled through the pile. The state in area 2, i.e., point 2 in the impedance diagrams, follows from Fig. 6, and serves as the starting point for this Fig. 7.

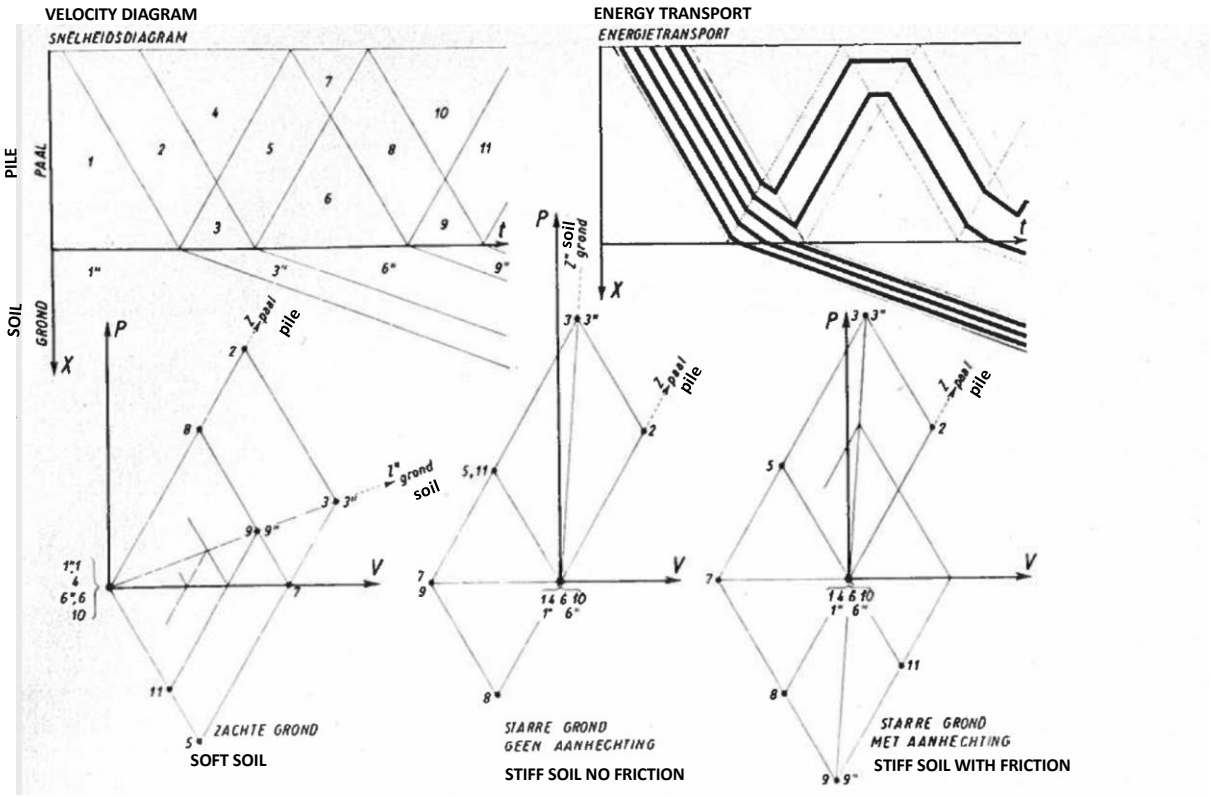

Figure 7:Stress wave in the pile reaches the toe, where the pile is in contact with soil, which is either less stiff or stiffer than the pile. The soil is schematized with a linear impedance Z"

The soil impedance *Z″* now determines the nature of the returning disturbance in the pile. The way the various intersecting points in the impedance diagram are generated is the same as in the preceding figure, and therefore does need to be discussed in detail here.

From the impedance figures for the 3 cases (soft soil and stiff soil with either a loosely supported pile toe (i.e., the pile can rebound) or a fixed pile toe), the expected tension stress in the pile can be assessed. In case of a soft subsoil, area 5 is already under tension, while for a stiff subsoil the tension only occurs from area 8 onwards. As tension is lost due to the soil friction along the pile shaft, it is to be expected that the stresses are smaller than indicated in the figure, since the stresses decrease with each passage of the stress wave through the pile. This means that e.g., point 5 will shift to the origin along the characteristic line for the pile and thus reduce the impedance figure.

In Fig. 7 the soil impedance is shown as a straight line *Z″*. We will see in the next section that due to the irreversible character of the deformation properties of sand, the impedance line becomes a zigzag line. It will also turn out that the energy transmission in sand, which is drawn in Fig. 7 as a straight bundle, has a different shape.

The calculation of the stresses and the velocity that exist at different times can be done with the aid of the diagrams, and shows e.g., that the magnitude of the stress wave in Fig. 6 can be described as

$$P_2 = \frac{V_1 Z Z'}{Z + Z'}$$

and the velocity, with which the drop hammer rebounds, as

$$V_3 = V_1 \frac{(Z - Z')}{(Z + Z')}$$

These graphically derived results can also be obtained mathematically.

We shall now move to the examination of the behaviour of sand, applying the method of characteristics developed here.

A 5. Propagation of a stress wave in sand

To simplify the analysis, we will consider the propagation of a stress wave in a cylindrical sample of dry sand. This sample is externally supported by a pressure along the entire circumference, on which the stresses mentioned below are deemed to be superimposed.

The deformation behaviour of the sample under the influence of further loading and subsequent unloading in the vertical direction is shown in Fig. 8a. It shows a smooth curved path with a sharp increase in the vertical shortening as the pressure reaches a certain limit value.

During unloading not all shortening is recovered. To graph the behaviour under the influence of a stress wave we will use the schematized dotted lines in Fig. 8a, i.e. during loading deformation moduli E_1 and E_2 for the stress increase from 0 to P_1 and from P_1 to P_2 respectively, and during unloading from P_2 to 0 a deformation modulus E_3. Due to the steepness of the unloading line E_3 is greater than E_1 and E_2, which means that under unloading the sand behaves as a stiffer material than under loading.

In the impedance diagram shown in Fig. 8b there are then 3 characteristic angles as the impedance for the sand column for these 3 states: $F\sqrt{E_1\varrho}, F\sqrt{E_2\varrho}$ and $F\sqrt{E_3\varrho}$ respectively.

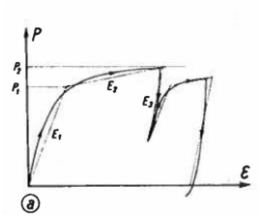

Figure 8a: The shortening of a sand cylinder under axial load shows a hysteresis loop

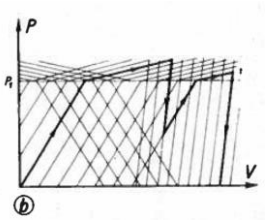

Figure 8b: Characteristic angles in the impedance diagram for the sand cylinder are different for loading and unloading and vary with the value of the stress P.

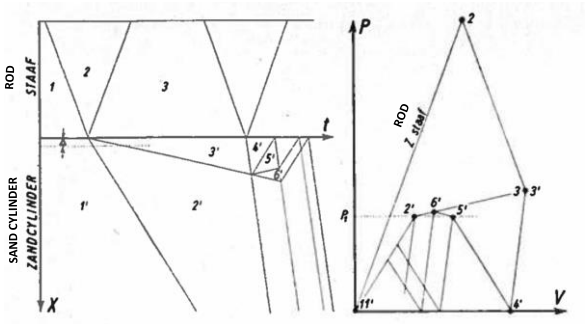

Figure 9: The stress wave reaches the interface between the sand cylinder and the rod. The triangular areas of stress increase in the velocity diagrams indicate limited penetration depth of the impact. The impedance diagram shows hysteresis loops.

In Fig. 9 the top of the sand cylinder is connected to a rod of equal diameter. With a drop hammer a stress wave is generated in this rod, which, similarly to what is shown in Fig 7, travels towards the interface between the rod and the sand cylinder. The magnitude of this stress wave in the rod is represented by point 2 in the impedance diagram shown in Fig. 9. Upon reaching the sand state 3 is established in the interface, which is determined by the impedance of the sand as per the segmented line 1'2'3'. In the velocity diagram this is reflected by the propagation of two pressure zones in the sand, in accordance with the characteristic angles for E_1 and E_2.This is self-evident considering what happens over time at a depth Δ below the interface (represented by the horizontal dotted line). First the pressure in the sand has to increase to *P1*, which occurs when transitioning from area 1' to 2'. When the pressure in the sand is P_1 the subsequent pressure increase to P_2 can only occur at a slower rate as $\sqrt{E_2} < \sqrt{E_1}$. Therefore the transition from 2' to 3' occurs later as the distance to the interface plane increases.

However, during unloading the pressure change occurs propagates faster because E_3 .is greater than E_2 and E_1 and therefore region 3' in the velocity diagram is truncated to a triangle at the transition to region 4'. The impedance diagram shows that 4' still has a positive velocity, which is greater than the velocity in area 2'. Due to this sand encroachment a wave runs back, which forms the boundary of area 4'. Fig. 9 is then developed further based on similar considerations and this generates points 5', 6' etc.. (For simplicity reasons it has been assumed in the drawing that no tensile stresses can be transmitted by the interface between the rod and the sand).

The line in Fig. 7 designated as Z"soil is replaced in Fig. 9 by the zigzag line 1'2'3'4'5'6' due to the irreversible properties of the sand. This zigzag line encloses the hysteresis loops in the PV diagram.

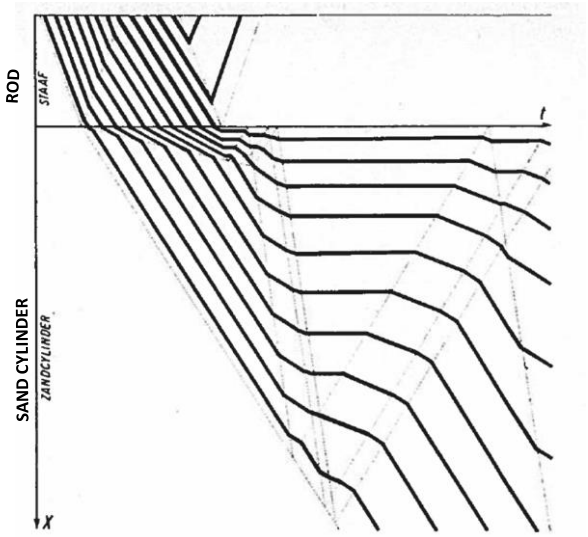

Figure 10: The lines representing the energy transmission in the sand gradually deviate towards the horizontal direction, indicating a loss of energy by conversion into frictional energy, which can no longer be recovered from the matter

The energy transmission is shown in Fig. 10, which resembles the velocity diagram of Fig. 9, but now with the energy lines shown. The family of lines in the sand must be viewed as smooth wavy lines since the kinks are due to segmented schematization in fig. 8a of the deformation theory.

The energy lines bend towards the horizontal direction, which means that energy remains in the sand, even when pressure and velocity have dropped to zero. This energy is equal to the frictional energy lost in the hysteresis loops described in the PV diagram.

Summary

The penetration of a stress wave into the sand cylinder reflects the characteristics of diffusion, because the higher stress levels propagate slower than the smaller ones. The unloading at the end of the stress wave propagates even faster, catching up with any pressure increase. As a result, the zone that experiences high stress levels is limited, but expands as the duration of the impulse increases.

In the end all energy lines in the energy transmission diagram will run horizontally, indicating that all energy in the matter is dissipated in the form of friction. The line spacing (when continuing Fig. 10 to the right) is the most dense at the top of the sand cylinder, which means that most of the energy will be dissipated there and that the resulting permanent deformations will therefore be greatest at the top of the sand cylinder.

A 6. Test Results

To demonstrate the theoretically obtained results with test data, Fig. 11 shows photographs of sand samples subjected to various forms of dynamic loads.

These are samples of uniform granules (0.1 to 0.3 mm), which are externally supported by a pressure of 0.4 kg/cm^2 on the enveloping membrane, which is the vacuum applied on the air in the pores. Originally the samples are almost 15 cm high and have a diameter of 3.8 cm (see photo a). The friction angle is approximately 27^o, so that the samples collapse under a vertical load of approximately 0.67 kg/m2.

When this load is applied statically (for a few seconds), the sample collapses in the manner shown in photo e, along two failure planes. Near the top and toe plates the sample is not deformed under the load in question, as these plates are rigid and provide the sample with additional support horizontally.

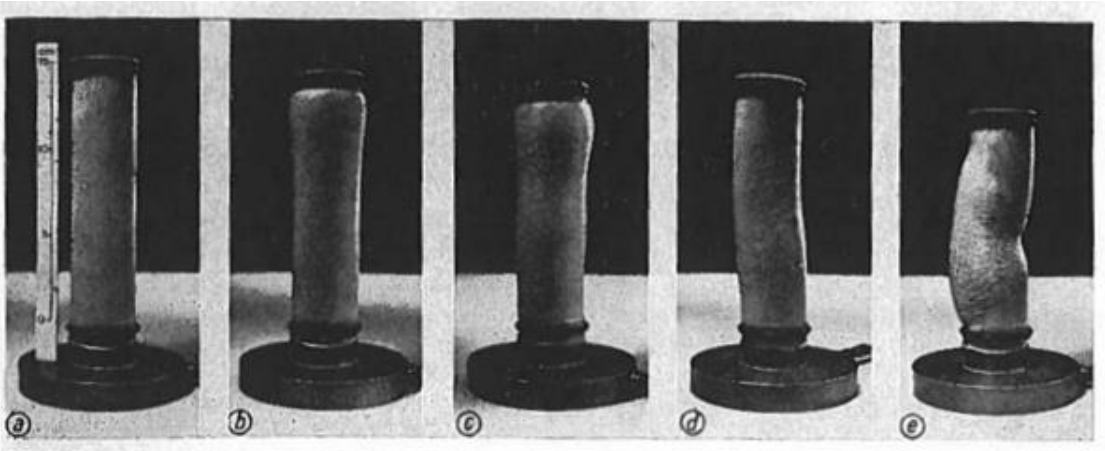

Figure 11: Different ways of loading a sand sample with an with impulse of 1 Ns
a: original sample, b, c, d: loading time 10^{-5} s, 10^{-3} s and 10^{-1} s respectively, e: static load.

Photographs b, c, d show the effect of a dynamic loading with a pulse of the same magnitude (1 N.s) in all three cases, but where the impact was applied in such a way that the loading time in photo b was approx. 10^{-5} s, in photo c approx. 10^{-3} s and in photo d approx. 10^{-1} s

As could be expected from the theory, the very brief impact (b) penetrates only slightly and the greatest permanent deformation is concentrated at the very top (despite the resistance of the rigid top plate). In case of c the maximum deformation is still at the top, but the action penetrates deeper as can be seen from the wrinkles in the rubber, which indicate the area where the sample has been compacted. In case of d the sample has been loaded uniformly over the full height. The image shows the characteristics of an extended static load. Finally in case of e the photo shows no deformation at the top plate and the beginning of the failure planes.

These images were obtained with drop hammers of widely varying composition and impedances to produce these extreme results.

We do not want to go any further into the lateral deformations at this time, but only mention that the exact theory for these failure forms is more complicated than calculated in the previous section, since the rotational waves cannot be neglected.

However, to demonstrate the differences of penetration depths depending on the duration of the impact, the examples are quite acceptable.

Conclusions

Due to its graphical nature the method of characteristics can provide a clear overview when impact problems are examined, whereby rods of different material and dimensions are interacting with each other. The propagation velocity and impedance of the rods determine the magnitude and duration of the forces that are generated.

When materials with irreversible properties are involved in the impact, the energy loss associated with the formation of permanent deformations is easily incorporated in the diagrams.

If a rod that is impacted rests with one end on a dry sand mass, then the shorter the impact duration the smaller the strongly disturbed zone.

B. Wave propagation in soil consisting of grains and water

The first part of the paper described how a dry granular material reacts to an impact load. For the geomechanical practice it is more important to study the behaviour of sand with water in the pores.

When developing the basic equation, not only the mass inertia and continuity of the two media must be considered, but also the friction that occurs when the two phases move relative to each other. To properly account for this last force, Darcy's law can be used, which states that the pressure drop in the pore water is equal to the water flow rate divided by the permeability coefficient k. This pressure gradient in water encounters its reaction in an equal but opposite force in the granular skeleton

B 1. Arrangement of the basic equations

Medium 1 is the water and at complete soil saturation it occupies n x the volume, where n = pore number.

Medium 2 are the soil granules that occupy the remainder: (1 -n) x the volume.

The two phases are then also distributed over the surface of any cross-section according to n and (1 – n).

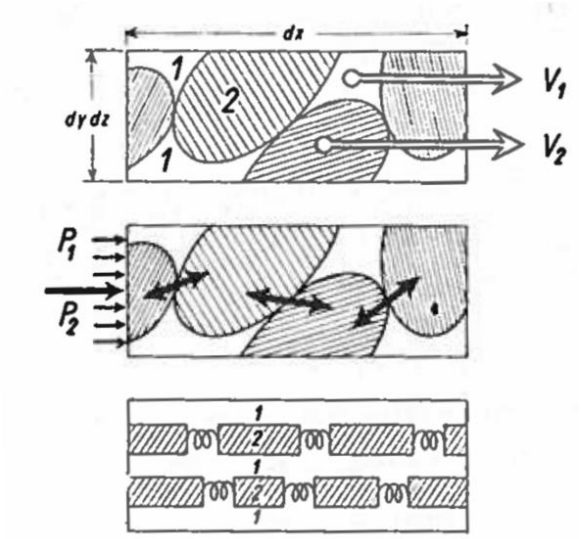

Figure 12:Velocity and stress distribution between soil granules and water

Figure 12 shows schematically how pressure and velocity are distributed over the two phases. The absolute velocities of water and grain are v_1 and v_2. The pore water pressure is p_1.

The effective soil stress p_2 is selected such that it is the average of the forces with which the soil granules rest on each other at the contact points. The total pressure on the soil granules in any cross-section *dy.dz* is then $p_2\,dydz + (1\text{-}n)\,p_1\,dydz$, *whereby* the second part of this expression reflects the water pressure on the granules. This total pressure acts on the granules' interior, but since the granules themselves are very rigid, there are no meaningful resulting deformations. However, the deformations observed externally on the skeleton are much greater and are the result of movements and indentation of the contact points. These are therefore related to the pressure p_2, and to simplify the calculation, we assume that the compression of the laterally confined skeleton is linear in accordance with $\epsilon = \frac{p_2}{K_2}$.

In the case of a polarized compression or expansion wave in the x-direction, the deformations and the derivatives of the various variables are equal to zero in the y- and z-directions.

The basic equations therefore only affect gradients in the x direction.

Equilibrium equations for the water

The mass of the water in volume *dxdydz* that must be accelerated is $\varrho_1 . n\,. dxdydz$, where ρ_1 is the density of the water. The required acceleration force is then $\varrho_1 . n \left(\frac{\delta v_1}{\delta t}\right) dxdydz$.

This force is the result of:
1) the pressure difference in the pore water over the distance dx, which is $-\left(\frac{\delta p_1}{\delta x}\right) n . dxdydz$;
2) the Darcy frictional force, which is equal to – (1/k) x water flow rate x *dxdydz*.

The water flow rate is the amount of water that moves relative to the granules through a cross-section per unit of time, divided by the total area of that cross-section. This can be described as is $n.dydz.(v_1 - v_2)/dydz$, and therefore the force on the water is – (n/k) $(v_1 - v_2)\,dxdydz$.

The equilibrium of forces then yields

$$n\varrho_1 \frac{\delta v_1}{\delta t} = -n\frac{\delta p_1}{\delta x} - \frac{n}{k}(v_1 - v_2) \qquad (1)$$

Equilibrium equation for the grains

The mass of the granules in volume *dxdydz* that must be accelerated is $\varrho_2 . (1 - n) . dxdydz$, where ρ_2 is the density of the granules. The required acceleration force is then $\varrho_2 . n \left(\frac{\delta v_1}{\delta t}\right) dxdydz$.

This force is generated by:
1) the pressure difference in the contact points of the granules over the distance dx, which is $-\left(\frac{\delta p_2}{\delta x}\right) . dxdydz$;

2) the water pressure, because the water exerts pressure on (1-n) of the surface area of the granules. This force is $-\left(\frac{\delta p_1}{\delta x}\right)(1-n)\,dxdydz$

3) by the Darcy frictional force, which acts opposite to that on the water, and is thus equal to $+\left(\frac{n}{k}\right)(v_1 - v_2)\,dxdydz$

The equilibrium of forces then yields

$$(1-n)\varrho_2 \frac{\delta v_2}{\delta t} = -\frac{\delta p_2}{\delta x} - (1-n)\frac{\delta p_1}{\delta x} + \frac{n}{k}(v_1 - v_2) \qquad (2)$$

Continuity equations for the water and granules

At the velocities that occur the volume of water in the volume dxdydz changes by $n\,dydz.\left(\frac{\delta v_1}{\delta x}\right)dxdt$ over time interval dt as a result of the water movement over part n of the surface, but at the same time the available volume of the water becomes smaller because the granules occupy the additional space

$$(1-n)dydz.\left(\frac{\delta v_2}{\delta x}\right)dxdt$$

This assumes rigidity of the granules, so that any variation in the volume of the skeleton must be at the expense of the water.

This volume reduction divided by the volume *n dxdydz* is equal to the pressure increase in the water $\left(\frac{\delta \varrho_1}{\delta t}\right)dt$ divided by the compression modulus of the water K_1, so that the continuity equation for th water becomes

$$\frac{\delta v_1}{\delta x} + \frac{\frac{1-n}{n}\delta v_2}{\delta x} - \frac{1}{K_1}\frac{\delta p_1}{\delta t} \qquad (3)$$

The value of p_2 for the granules has been selected such the continuity equation can be written directly as:

$$\frac{\delta v_2}{\delta x} = -\frac{1}{K_2}\frac{\delta p_2}{\delta t} \qquad (4)$$

B 2. Propagation of a harmonic oscillation with frequency w

In order to examine the dynamic phenomena that eqs (1), (2), (3) and (4) provide grounds to do, a look into the effect is of a harmonic oscillation with frequency ω will be meaningful.

In section C2 we will explain how the results of calculations for harmonics are used in the study of impacts. For now let us just state that the solution is the complex oscillation

$$v_{1,2}(xt) = \tilde{v}_{1,2}\, e^{i\omega\left(t-\frac{x}{c}\right)} \qquad (5)$$

which propagates with a velocity *c* in the x-direction.

Elimination of p_1 and p_2 from eqs. (1), (2), (3) and (4), and combining them with (5) results in the following equation for the exponents of e:

$$\left[-K_1\frac{\omega}{c^2} + \varrho_1\omega - \frac{i}{k}\right]\tilde{v}_1 = \left[\frac{1-n}{n}\,K_1\frac{\omega}{c^2} - \frac{i}{k}\right]\tilde{v}_2$$

$$\left[-(1-n)\varrho_1\omega - \frac{i}{k}\right]\tilde{v}_1 = \left[\,K_2\frac{\omega}{c^2} - (1-n)\varrho_2\omega + \frac{i}{k}\right]\tilde{v}_2 \qquad (6)$$

As these two equations cannot conflict with each other, the following 4th order equation can be formulated for c:

$$c^4\left[\frac{(1-n)\varrho_1\varrho_2}{K_1K_2} + \frac{1}{i\omega k}\frac{n\varrho_1 + (1-n)\varrho_2}{K_1K_2}\right] - c^2\left[\frac{(1-n)\varrho_2K_1 + (1-n)^2\varrho_1K_1 + n\varrho_1K_2}{nK_1K_2}\right. + \frac{1}{i\omega k}\cdot\left(K_1 + \frac{nK_2}{nK_1K_2}\right] + 1 = 0$$

Which be shortened by introducing α and ß as

$$\alpha^4c^4 - \beta^2c^2 + 1 = 0 \qquad (7)$$

From eq. (7) the propagation velocity c can be derived, resulting in 4 values:

$$c = \pm\frac{1}{\alpha\sqrt{2}}\left[\left(\frac{\beta^2}{2\alpha^2}+1\right)^{\frac{1}{2}} \pm \left(\frac{\beta^2}{2\alpha^2}-1\right)^{\frac{1}{2}}\right]$$

The first ± sign refers to the direction of propagation, i.e., in ± x direction. The second ± sign yields two different values for c, which appear more easily by considering that $\beta^2\alpha^2$ is much more than 1 for typical property values that apply to wet sand:

ρ_1 = 1000 *kg/m* ρ_2 = 2500 *kg/m* n = 0.25 -0.5
k = 10^{-9} m^4/N.s (for v < 10^{-3} cm/s)

For frequencies above 1000 Hz. there are then two approximate propagation velocities *c'* and *c"*:

$$c' = \frac{\beta}{\alpha^2} = \sqrt{\frac{\left[\left(\frac{K_1}{n}\right)+K_2\right]}{[n\varrho_1+(1-n)\varrho_2]}}$$

$$c'' = \frac{1}{\beta} = \sqrt{\frac{i\omega k}{\frac{1}{K_1}+\frac{1}{nK_2}}} = (1+i)\sqrt{\frac{\omega k}{2\left(\frac{1}{K_1}+\frac{1}{nK_2}\right)}} \quad (8)$$

The physical significance of this outcome becomes clear when one considers the stress distribution between water and the granules.

B 3. Distribution of stresses over water and grains

To demonstrate what happens when the soil is dynamically loaded, we will examine how the stresses are distributed over the two constituent, when at the location of x = 0 only the granules are loaded with an alternating stress (with frequency ω) and thus the water remains unloaded at that location so

$$p_1 = 0 \text{ and } p_2 = pe^{i\omega t} \text{ for x = 0} \qquad (9)$$

Since there are two rates of propagation, the solution for v_1 and v_2 also consists of two parts:

$$v_1(x,t) = \tilde{v}_1' e^{i\omega\left(t-\frac{x}{c'}\right)} + \tilde{v}_1'' e^{i\omega\left(t-\frac{x}{c''}\right)}$$
$$v_2(x,t) = \tilde{v}_2' e^{i\omega\left(t-\frac{x}{c'}\right)} + \tilde{v}_2'' e^{i\omega\left(t-\frac{x}{c''}\right)} \quad (10)$$

The ratios $\tilde{v}_1'/\tilde{v}_2'$ and $\tilde{v}_1''/\tilde{v}_2''$ can now be calculated by entering in one of the eqs. (6) the values of resp. *c'* and *c"* derived from eq. (8). It then appears that, when the practical values are used, the following ratios for the various velocities have a high degree of accuracy:

$$\tilde{v}_1' = \tilde{v}_2' \qquad (11)'$$

$$\tilde{v}_1'' = \tilde{v}_1''\left(\frac{1-n}{n}+\frac{K_2}{K_1}\right) \qquad (11)''$$

One can now enter the velocities according to eq (10) and eq. (11) in eq. (3) and eq. (4) and thus express the stresses p_1 and p_2 e.g. as a function of v_1' and v_1'', and then calculate the values of v_1' and v_1'' as a function of the stress amplitude *p,* using the boundary condition listed at (9). This generates the following expressions for the stresses:

$$p_1 = \frac{p}{\left[\left(\frac{K_1}{n}\right)+K_2\right]}\left[\frac{1}{n}K_1 e^{i\omega\left(t-\frac{x}{c'}\right)} - \frac{1}{n}K_1 e^{i\omega\left(t-\frac{x}{c''}\right)}\right]$$
$$p_2 = \frac{p}{\left[\left(\frac{K_1}{n}\right)+K_2\right]}\left[K_2 e^{i\left(\omega t-\frac{x}{c'}\right)} - \frac{1}{n}K_1 e^{i\omega\left(t-\frac{x}{c''}\right)}\right] \quad (12)$$

B4. Discontinuous load change on impact

The foregoing result of an oscillation with frequency ω on a mixture of granules and water can be used conveniently to determine the influence of a sudden pressure change. A discontinuous load increase of *P* at *t* = 0 can be described as a summation of harmonic oscillations using the Fourier integral:

$$P(t) = \frac{P}{2\pi}\int_{-\infty}^{\infty}\left(\frac{1}{i\omega}\right)e^{i\omega t}\,d\omega \qquad (13)$$

The replacement of the boundary condition (9) by expression (13) has the same effect on the results expressed by eqs. (12) as the inversion

integral in calculus, where the imaginary variable $i\omega$ replaces the real variable s in the Laplace transform.

Calculation of the distribution of the stresses over water and the granules according to eq. (12) then requires the inversion of the functions:

$$\frac{1}{s}e^{-\frac{sx}{c'}} \; and \; \frac{1}{s}e^{-\frac{sx}{c''}} = \frac{1}{s}e^{-\frac{x}{\sqrt{Ks}}}$$

where

$$c' = \sqrt{\frac{\left[\left(\frac{K_1}{n}\right) + K_2\right]}{[n\varrho_1 + (1-n)\varrho_2]}}$$

$K = \frac{kK_1K_2}{\left[\left(\frac{K_1}{n}\right)+K_2\right]}$ (≈consolidation coefficient).

The inversion is known from the Laplace Theory and generates in the end the following for the stresses:

$$p_1 = \frac{K_1}{K_1 + nK_2} P \left[\begin{Bmatrix} 0 \; if \; t < \frac{x}{c'} \\ +1 \; if \; t > \frac{x}{c'} \end{Bmatrix} - K - \begin{Bmatrix} 0 \; if \; t < 0 \\ erfc\left(\frac{x}{2\sqrt{Kt}}\right) if \; t > 0' \end{Bmatrix} \right] \qquad (14)$$

$$p_2 = \frac{K_1}{K_1 + nK_2} P \left[\frac{nK_2}{K_1} \begin{Bmatrix} 0 \; if \; t < \frac{x}{c'} \\ +1 \; if \; t > \frac{x}{c'} \end{Bmatrix} + \begin{Bmatrix} 0 \; if \; t < 0 \\ erfc\left(\frac{k}{2\sqrt{xt}}\right) if \; t > 0' \end{Bmatrix} \right]$$

Figure 13 displays pressure curves in accordance with eqs. (14).

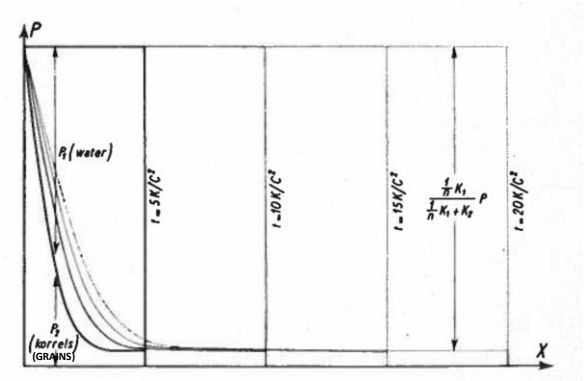

Figure 13: Impact loading of the granules at x = 0 causes a rapid acoustic propagation of pressure in pore water followed by slow adjustment of grain pressure

B 5. Physical interpretation of eqs. (12) and (14)

Let us first consider the second term in brackets in all expressions. Due to the complex value of *c"* (see eq. (8)) this term quickly dampens the stresses during a harmonic oscillation. (The distance *x*, for which the amplitude is reduced to *1/e*, becomes smaller than 2 cm, for frequencies greater than 1000Hz and normal values for sand $k = 10^{-9}$ m^4/N.s, $K_2 = 10^8$ N/m^2).

For the impact load, the second term is an error integral:

$$erfc(z) = 2\pi - \frac{1}{2}\int_z^{\infty} \exp(-\lambda^2) \; d\lambda$$

which describes the consolidation phenomenon, according to which the pore pressures in the interior are relieved at the edge of the soil body. The value of this term is 1 for *x* = 0 and decreases rapidly with distance x. (The distance x, for which half the consolidation has taken place, is approximately $20\sqrt{t}$ cm, where t is the loading duration in seconds for practical values for sand).

In both expressions, the second term has the effect of a rapidly attenuated perturbation at the edge, which provides the boundary condition that the pore pressure is zero for x=0.

If we then consider the first term, we see that the ratio of the terms for water and granules is $K_1/n : K_2$. Since the compression modulus for water K_1 is much greater than that for the granules K_2, the total amplitude p at the harmonic oscillation and the total force P in case of instant loading are distributed over the granules and water in such a way that water assumes the largest share.

From the formulation of the first term we further see that it represents a phenomenon, which propagates with a velocity c'. The concept of this propagation velocity according to eq. (8) now becomes more manageable. In the derived stress distribution the numerator $\mathrm{K}_1/\mathrm{n} + \mathrm{K}_2$ represents the compression modulus of the soil component, while the denominator is equal to the density of this component. Thus the value of c' is thus reduced to the usual form $c' = \sqrt{K/\rho}$ for the propagation of a compression wave in a homogeneous medium, where K is the constrained compression modulus and ρ the density.[3]

From eq. (11)' we see that the first term refers to movements of the granules and water, which occur in the same direction and are equal in value. So, it is understandable that as part of this movement the water, which is the stiffest, assumes most of the force. According to (11)'' the second term consists of opposite movements of the granules and water, which is why the Darcy friction is maximum for this part and results in rapid damping.

We thus obtain the following image when compaction waves are generated in a sand body: within a very short distance practically the entire force is assumed by the water, even though the granules are loaded initially. This water pressure propagates at a high speed, which is almost equal to the speed of sound of water and in the order of 1000 m/sec. is. In a dilation wave, water and grains move together as a whole.

Since the pressure in the granules is so small compared to that in the water, the influence of the typical material properties of the sand (non-linearity and irreversibility) on the entire course of the phenomenon is very small, and when it comes to dilation waves, the water-saturated soil behaves like an elastic medium with the compressibility of water and the density of the soil.

The soil behaves completely differently when it comes to rotational waves.

B 6. Rotational Waves

The foregoing dealt with dilation waves. This wave consists only of movements of matter in the wave propagation direction and contains no rotations. Apart from that type of waves, rotational waves can also occur in a soil body. These waves consist of movements perpendicular to the propagation direction and do not involve any compaction of matter. Generally speaking, in case of a dynamic phenomenon in a soil body, both wave types must be considered in order to be able to satisfy the boundary conditions.

In addition, each wave phenomenon can only be described as a combination of dilatation and rotational waves. Since in a rotational waves no densification of matter occurs, it is to be expected that the pore water pressures in the soil with this wave type are negligible. We will not prove this in detail here, but simply state the conclusion that practically the entire rotational wave is absorbed by the granular skeleton and therefore all characteristic properties of dry sand are observed in case of a rotational wave in wet

[3] In the calculations of c in paragraph B2 a minor aspect is neglected, which means that in reality c' has a very small imaginary component, which causes a small damping effect.

sand. The propagation speed of the rotational wave is $\sqrt{G/\rho}$, where *G* is the sliding modulus of the granular skeleton and ρ the density of the mixture of granules and water. The value of *G* should take into account the non-linear and irreversible character of sand.

In loosely packed sand with a less than critical density, the rotational waves cause such shifts in the granular skeleton that the granules start to float. With every loading and unloading cycle more contact points are then broken, so that especially oscillations with many successive load changes can really emphasize this effect.

C. Effect of the geometric spread of a impact around a pile tip

To describe the three-dimensional character of the impact extension below the pile toe, we only have a calculation that applies to an elastic infinite soil body, whereby the pile toe is schematically shaped as a sphere. For this reason, we cannot use the outcome for the permanent deformations in the sand and neither has the local collapse along failure planes been taken into account.

The outcome is, however, insofar meaningful that it gives us an impression of the pressure distribution between granules and water, since the impedance experienced by the sphere from the solid can be split into a dilatation and a rotation component.

If the displacements u_r and u_z, are stated in polar coordinate directions as derived from two functions *E* and Ω as

$$2Gu_r = (1-2\nu)\left(\frac{\delta^2 E}{\delta r \delta z}\right) - 2(1-\nu)\left(\frac{\delta^2 \Omega}{\delta r \delta z}\right)$$

$$2Gu_r = (1-2\nu)\left(\frac{\delta^2 E}{\delta z^2}\right) - 2(1-\nu)\left(\frac{r^{-1}\delta}{\delta r\left[\frac{r\delta\Omega}{\delta r}\right]}\right)$$

then the increase in volume *e* and the rotation ω_{rz} are given by

$$2Ge = (1-2\nu)\frac{\delta(\nabla^2 E)}{\delta z}$$

$$2G\omega_{rz} = (1-\nu)\frac{\delta(\nabla^2 \Omega)}{dr}$$

A solution for these differential equations for the dynamic equilibrium at frequency ω can be the following set of functions:

$$E = AR^{-1}\exp(-\alpha R + i\omega t)$$

$$\Omega = BR^{-1}\exp(-\beta R + i\omega t)$$

with

$$\alpha = i\omega\sqrt{(1-2\nu)\frac{\rho}{2}(1-\nu)G} = i\omega\sqrt{\frac{\rho}{K}}$$

$$\beta = i\omega\sqrt{\frac{\rho}{G}}$$

With a correct choice of the integration constants A and B, these two equations for *E* and Ω are adequate to satisfy the boundary conditions imposed on an infinite soil body that is loaded by a rigid sphere in the Z direction. with an alternating force $Pexp(i\omega t)$.

After elaboration according to the Theory of Elasticity, the derived impedance, experienced by the sphere due to the soil body, is

$$\frac{P}{\frac{\delta u_z}{\delta t}} = \frac{4\pi G R_0}{i\omega}\cdot \frac{\left\{\begin{array}{l}(1+\alpha R_0)(3+3\beta R_0+\beta^2 R_0^2)\\ +2(1+\beta R_0)(3+3\alpha R_0+\alpha^2 R_0^2)\end{array}\right\}}{\left\{\left(\frac{\alpha^2}{\beta^2}\right)(3+3\beta R_0+\beta^2 R_0^2)+2(3+3\alpha R_0+\alpha^2 R_0^2)\right\}}$$

where R_o is the radius of the sphere.

The first term enclosed in the braces in the numerator is the dilatation portion, while the second term covers the rotation, which in line with the foregoing means the portion of the pressure assumed by the water and the portion taken up by the granules respectively.

For high values of the frequency ω, the ratio between these two terms is $\beta: 2\alpha = \sqrt{K}: 2\sqrt{G}$, which means that the water assumes most of the pressure since *K >> G.*

At low frequencies the ratio is 1:2, so that the granules then assume 2/3 of the total force.

High frequencies are those, for which $\omega \gg \sqrt{\frac{K}{\rho R_0^2}}$. As shown in Fig 14b the impedance can then be modelled as a dashpot $D_0 = 4\pi R_0^2 \left(\frac{1}{3}\sqrt{\rho K} + \frac{2}{3}\sqrt{\rho G}\right)$, which represents the acoustic emission of the spherical surface, followed by a mass $M = \frac{4}{3}\pi R_0^2 \rho$, to represent the displaced soil.

Low frequencies are those, for which $\omega \ll \sqrt{\frac{G}{\rho R_0^2}}$. As shown in Fig 14a the impedance can in that case be modelled as a spring with stiffness $S = 4\pi G R^2 [\frac{6(1-\nu)}{5-6\nu}]$, which corresponds with the static compression of a sphere in an infinite soil body.

Using the above calculation, it is possible to determine all stresses and displacements in the soil body surrounding the sphere. However, due to length limitations these results are not reported here. Due to the terms $R^{-1}\exp(\alpha R)$ and $R^{-1}\exp(\beta R)$ in the original functions, the stresses propagate along spherical wave fronts and decrease with distance R. For ω approaching 0, these stresses morph into the distribution Stokes calculated around a sphere moving through a liquid.

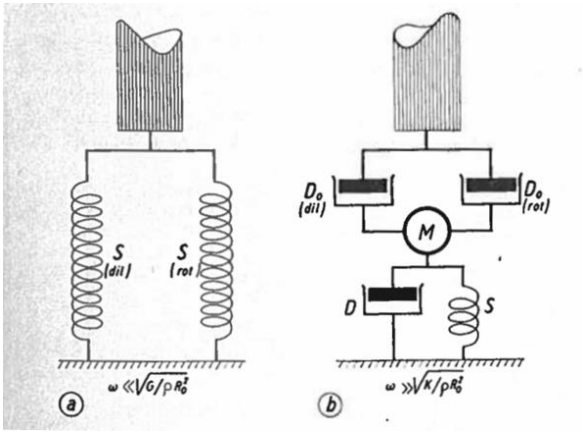

Figure 14: .Schematic of the impedance experienced by the pile toe from the soil at (a) low and (b) high frequencies.

Conclusion

Various aspects, which make the dynamic nature of loading during pile driving different from a static load, have been made explicit through calculations.

Some conclusions that can be drawn from the physical interpretation of the results are the following:

a. A load of very short duration has limited penetration depth insofar as it irreversibly deforms the granular skeleton of a sand body. If the loading lasts longer, the zone of permanent deformations is more extensive, and the method of loading resembles more closely that associated with a static load. In dry sand this applies to compaction and rotational formations, while in water-saturated sand it really applies only to the rotational wave.

b. In water-saturated sand no compaction deformation occurs during short-term loading, because the water assumes all the pressure. The water pressure expands into the surroundings in the form of a compression wave and propagates at high speed, without significantly deforming the granular skeleton.

As the load lasts longer, the granules once again assume the stresses from the water.

c. The pile toe, schematically shaped into a sphere, experiences more resistance from the

surrounding soil in the form of compression waves as the loading frequency increases.

Since these compression waves result in minimal permanent deformations of the granular skeleton, the energy that goes into it is of no use during pile driving. The generation of high-frequency oscillations in the pile occur in the pile driving helmet and can be avoided by making the right choice for the impedances of the ram, pile helmet and pile. With the diagrams in chapter A it is possible to calculate whether e.g. the pile helmet will begin to rattle between the ram and the pile, or whether the blow has a penetrating effect.

An impact that lasts for a long time, develops rotational waves that affect the granular skeleton. The longer it lasts, the greater the penetration depth and the smaller the force required to penetrate the pile over a certain distance. The impulse, which is distributed over a longer period, creates less stress in the pile and causes greater penetration. This consideration may be useful when examining pile fractures during pile driving.

In cases where the sand has a lower density than the critical one, the occurrence of vibrations can actually increase the pore pressures and therefore a reduction of the resistance. Since the impact duration depends on the wave propagation velocities in the ram, pile helmet and pile (and in some situations also on the ratios of these impedances), all these quantities should be taken into account as well to draw conclusions regarding the soil properties from the blow counts during the pile driving.

The dynamic character of the loading is lost the longer the impact lasts. Since the diffusion velocity for the pore pressures and the penetration depth of the impact differ for different types of soil, the impact duration, which can be regarded as static, is not the same everywhere.

It seems that for a 15 cm high dry sand sample a blow of 0.1 sec. can be regarded as a completely static load.

The dimensions of the CPT cones and the velocity of pushing rate during a sounding are such that one can always speak of a test method equivalent to a static load test.

It is not inconceivable that the impact ram and impact face on a bar are dimensioned in such a way, that under certain circumstances a drop test can also be regarded as a static loading.

References:

[1] N. NANNINGA:”Het heiproblecm", (The pile driving problem) ,*De Ingenieur* nr 42, 1953.
[2] J. Massau: „Memoire sur l'integration graphique des equations aux derivees partielles'',(Memoir on the graphical integration of partial differential equations''). Mons. 1914.
[3] J. C. SCHONFELD: „Voortplanting van getijden en soortgelijke golven", (Propagation of tides and similar waves, thesis), dissertatie. Delft 1951.
[4] R. Sauer: „Anfangswertprobleme bei partiellen Differentialgleichungen", (Initial value problems in partial differential equations), Berlin 1952.